BULLETIN OF THE POLISH ACADEMY OF SCIENCES
TECHNICAL SCIENCES, Vol. XX, No. Y, 2018
DOI: 10.1515/bpasts-2018-00ZZ

Deep learning versus classical neural approach to mammogram recognition

J. KUREK[1], B. SWIDERSKI[1*], S. OSOWSKI[2], M. KRUK[1], W. BARHOUMI[3]

[1]Faculty Of Applied Informatics and Mathematics, Warsaw University of Life Sciences,166 Nowoursynowska Street, 02-787 Warsaw, Poland
[2]Faculty of Electrical Engineering, Warsaw University of Technology and Faculty of Electronic Engineering, Military University of Technology, Warsaw, 75 Koszykowa Street, 00-662 Warsaw, Poland
[3]Research Team on Intelligent Systems in Imaging and Artificial Vision (SIIVA)- LimTic Laboratory, ISI, University of Tunis El Manar, Tunisia

Abstract. Automatic recognition of mammographic images in breast cancer is a difficult problem due to confusing appearance of some normal tissues which look like masses. The existing computer-aided systems suffer from non-satisfactory accuracy of cancer detection. This paper copes with this problem and proposes two alternative techniques of mammogram recognition: the application of many different methods for definition of the numerical descriptors of the image in combination with an efficient SVM classifier (so called classical approach) and application of deep learning in the form of the convolutional neural networks, enhanced with the additional transformations of the input mammographic images.

The key point in the first approach is defining the proper numerical descriptors of the image and selecting the set which is the most class discriminative. To achieve better performance of the classifier, many descriptors of images were defined by applying different characterization of the images: Hilbert curve representation, Kolmogorov-Smirnov statistics, maximum subregion principle, percolation theory, fractal texture descriptors as well as application of wavelet and wavelet packets. Thanks to them better description of the basic properties of the image has been obtained. In the case of deep learning the features are automatically extracted in convolutional neural network learning. To get better quality of results the additional representations of mammograms in the form of nonnegative matrix factorization and self-similarity principle have been proposed. The applied methods were evaluated on a large database composed of 10168 regions of interest of mammographic images taken from the DDSM database. Experimental results prove the advantage of the deep learning over traditional approach to image recognition. Our best average accuracy in recognizing abnormal cases (malignant plus benign versus healthy) was 85.83%, sensitivity 82.82%, specificity 86.59% and AUC=0.919. These results belong to the best for this big data base.

Key words: convolutional neural networks, breast cancer diagnosis, mammogram recognition, diagnostic features.

1. Introduction

Breast cancer belongs to the most dangerous cancer affecting women. More than 18% of all cancer deaths, including both males and females, are from breast cancer. Over 1.67 million new cases worldwide in 2012 have been registered [1]. The early detection of cancer is crucial for treatment, since it means better perspective of recovery.

The screening mammography programs are organized to cope with the problem and to reduce the mortality rate [2,3]. However, the mammography interpretation is a difficult task due to the subtle signs of breast abnormalities, which could be observed in an early stage. According to statistics, 10-15% of cancer cases are undetected.

Due to the huge amount of screening mammograms, which should be analyzed by two independent experts and due to the limited number of expert radiologists, it is a bottle neck in all screening programs. Therefore, the Computer Aided Detection (CAD) systems are urgently needed. Such system can replace the second reader and alert the expert radiologist to the suspicious regions. However, the accuracy of the actually developed systems is still not satisfactory. Different solutions have been reported to the computer aided mammogram recognition. They differ by image preprocessing stages, which lead to different diagnostic features and also by the solution of classification systems used in the recognition of pattern formed by these features.

The paper [4] reviews different methods of feature definition and application of the classification tools. The diagnostic features are based on characterization of the texture, edge orientation, statistical analysis of a map of pixels in the mammographic image, etc. Different mathematical tools are used in definition of the features. They include wavelet decomposition, mathematical morphology, thresholding methods, template matching, neural networks and many others. The paper [4] presents the comparison of actual results of different approaches to recognition of normal from abnormal mammograms, obtained for limited number of mammograms (from 128 to 280). However, the quality factors defined in the form of true positive rate TPR= 75.7%, false positive rate FPR=73.5% and AUC (area under ROC curve) changing for different solutions from 0.76 to 0.89 were not satisfactory. The paper [5] has presented application of extreme learning machine to the tumor detection in double views mammography.

Most research presented in literature used only small database of mammographic images. The paper [6] has presented the application of principal and independent component analyses for generation of diagnostic features and radial basis function network as a classifier. The accuracy rate of 88.23% in detection of all kinds of abnormalities in the analyzed 119 regions of suspicion for mammogram images in Mini Mammographic

Database of MIAS has been reported. In [7] the features based on estimation of the probability density function of the gray level differences in the image were defined. After genetic algorithm and forward sequential selection these features have been used as the input signals to the multilayer perceptron used in the classification mode. The classification accuracy of 89%, with 88.6% sensitivity and 83.3% specificity have been reported for 410 mammograms from Digital Database for Screening Mammography (DDSM). The 600 cases taken from DDSM were analyzed in [8] using three different methods of feature problem solution: genetic algorithm, greedy selection and random mutation hill climbing. Different commercial CAD products for mammography analysis, including AccuDetect Parascript® [9], R2 ImageChecker and iCAD Second Look [10] have been checked in recognizing the abnormal cases. It was shown, that all of them suffer from the limited accuracy. The best results of AUC was 0.789.

In [11] the recognition results of abnormality cases in all mammograms of DDSM base by using the curvelet moments was presented. Only the accuracy rate was reported It changed from 81.26% to 86.46% depending on the applied feature set. However, no sensitivity, specificity and AUC information have been presented. In [12] the application of deep learning to the recognition of mammograms was proposed.

The aim of this work is to develop and compare two new approaches to mammographic image recognition, able to recognize the abnormal cases (benign +malignant) from normal, with an increased accuracy. Both will be used to analyze the regions of interest (ROI) of the mammograms. The first approach consists in typical steps used in classical pattern recognition: generation of numerous numerical descriptors of the image, selection of the most discriminative ones, which will serve as the diagnostic features for classifier and final classification step by using the support vector machine (SVM). To get the most objective and independent description of the image we have proposed different feature extraction methods. They include representation of the image by Hilbert curve and definition of spe**c**ial descriptors based on the self-similarity of vectors, Kolmogorov-Smirnov statistics, maximum subregion principle, percolation theory, the gray level co-occurrence matrix (GLCM) analysis, fractal texture description as well as application of wavelet and wavelet packets in creating numerical descriptors. To the best of our knowledge most of them are applied for the first time in mammographic image analysis. In the next step a sequential feature selection method is used to choose the most class-discriminative subset of features. In the classification step the SVM has been applied.

In the second approach we will use the deep learning strategy based on the convolutional neural network (CNN) as the work horse. CNN plays the role of the unsupervised feature selection and a final classification at the same time. However, direct application of the set of mammograms available in DDSM base to the CNN is not fully successful due to the limited number of the sample images. Therefore, we propose to expand the input data by the additional images created by applying the non-negative matrix factorization (NMF) and statistical self-similarity. They fulfill the significant role in the classification system and allow increasing the accuracy of the image recognition.

The numerical experiments have been performed on a large DDSM data base containing more than 10000 mammograms. The results of these investigations have confirmed good accuracy of class recognition. The comparison of the classical and deep learning approaches has shown the advantage of deep learning strategy. The main contribution of this work is as follows:

- Proposition and application of novel methods for extracting the numerical descriptors of the mammographic images in classical neural approach to image recognition. Diversity of descriptions allows characterizing details of the images from many different points of view.
- Successful application of deep learning strategy in the form of convolutional neural network to the analysis of mammographic image. The important element in this representation is an application of the non-negative matrix factorization and statistical self-similarity, which are able to enhance the differences between classes of mammograms and in this way increase the accuracy of class recognition.
- An experimental evaluation of the proposed solution on the DDSM set of mammograms and proving its better performance in comparison to other results presented actually in different papers. Our best average accuracy in recognizing abnormal cases from normal was 85.83%, sensitivity 82.82%, specificity 86.59% and AUC=0.919. These results are one of the best for this set.

The rest of the paper is organized as follows. Section 2 describes shortly the database of the used mammograms. Section 3 presents the classical approach to image recognition and the results of the numerical experiments. Section 4 is devoted to the deep learning approach to mammogram recognition. Section 5 compares the obtained results using both methods and the other reported in actual publications. The concluding section summarizes the presented considerations.

2. Database of mammograms applied in investigations

The numerical investigations have been carried out using the largest publically available database of mammographic images “Digital Database for Screening Mammography”[13]. It is composed of 2604 cases, each containing 4 mammograms (left and right breast from

above representing Cranial-Caudal view and oblique representing Medio-Lateral-Oblique view). The dataset contains the important information of each mammogram, including its diagnostic results (normal, benign or malignant) and the location of existing lesions forming ROI. For the abnormal cases (benign and malignant), a manual cropping was done based on the information provided in the ground truth. The ROI corresponding to masses represents rectangular area with the lesion in the center. In normal cases ROI was extracted manually by the medical expert from normal tissues. The size of ROI images was the same and equal 128×128 pixels, irrespective of its type. The number of ROI images, that has been used in experiments was 10168. The DDSM data base contained the following number of class representations:

a. Normal tissue: 8254,
b. Benign lesion: 862,
c. Malignant lesion: 1052.

It means that the abnormal tissue set representing the benign and malignant cases contains only 1914 ROI images, much less than normal ones (8254 samples). It presents some additional problems related to the unbalanced set of data.

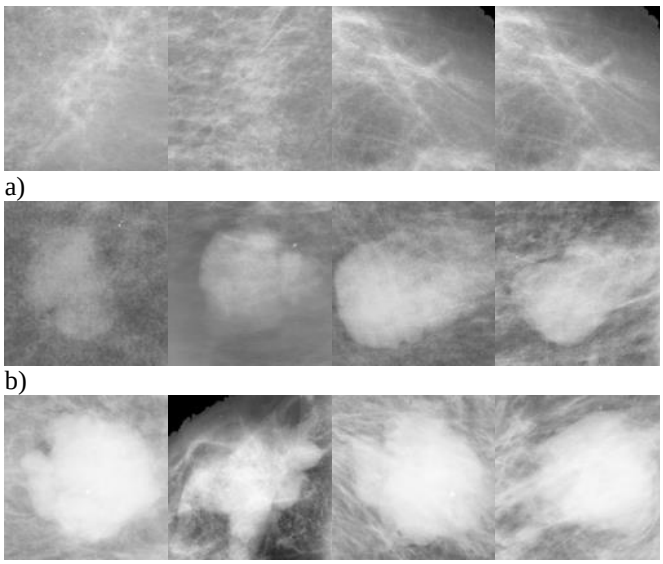

a)

b)

c)

Fig. 1 The ROI examples of mammograms representing normal (a), benign (b) and malignant (c) cases.

This problem was solved by splitting the set of normal cases into 4 subsets, each confronted in classification with the same set of abnormal cases and applying the majority voting rule.

Fig. 1 presents the examples of mammograms of normal (Fig. 1a) and abnormal cases: benign (Fig, 1b) and malignant (Fig. 1c). We can observe the significant differences among the images representing the same class of data and close similarity of images representing different classes. It results in significant problems on the stage of class recognition.

3. Classical neural approach to mammogram recognition.

Three independent steps are usually applied in the classical neural approach to image recognition: extraction of the numerical descriptors of the images, selection of the best set of the class discriminative diagnostic features and the classification step responsible for the final recognition of classes.

3.1 Definition of numerical descriptors of the mammographic images

The main problem in efficient numerical characterization of the mammographic images is their diversity inside the same class of images and close similarity between the normal and abnormal tissues. To cope with this problem we propose application of different mechanisms of feature definition, characterizing the image from different points of view. The applied methods will refer to characteristics of chaotic systems using fractal measures, texture description using the co-occurrence Haralick's matrix and Kolmogorov-Smirnov statistics, self-similarity of images, percolation theory, different types of statistical description as well as description based on wavelet representation. In generating the image numerical descriptors the following methods are used

- description based on Hilbert's curve representation of the image,
- statistical description based on coaxial rigs image representation and their characterization by applying Kolmogorov-Smirnov distance,
- maximum subregion principle,
- description based on percolation theory,
- texture description based on the gray-level co-occurrence matrix,
- application of self-similarity principle of the image in connection with box-counting dimension,
- segmentation-based fractal texture analysis,
- application of wavelet and wavelet packet decomposition.

3.1.1 Kolmogorov-Smirnov descriptors

Kolmogorov-Smirnov (KS) descriptors belong to the statistical parameters. They are defined on the basis of pixel intensity in the coaxial rings of the increasing diameters [14]. The succeeding regions of the image are split into few concentric rings around the central point The particular regions contain approximately equal number of pixels in each ring. The central point is traveling around the whole image. In each position of it the KS statistics describing the difference between the

pixel populations in the rings placed in equal distances from each other are estimated. The KS statistics checks if the pixels belonging to two rings are belong to the same population. KS distance is defined on the basis of their cumulative distributions $F(x_i)$ and $F(x_j)$

$$d_{KS} = \max \left| F(x_i) - F(x_j) \right| \quad (1)$$

over all x. This distance represents the measure of difference between the pixel statistics in both rings.

Four coaxial rings have been constructed for each mammographic image. Every coaxial ring contains approximately the same number of pixels. The set of KS distances corresponding to the combinations of these four levels have been estimated. Level 1 represents KS distance of two succeeding rings, i.e., rings 1 and 2, 2 and 3, 3 and 4, etc. Level 2 describes the statistics of rings distant by 2, for example 1 and 3, 2 and 4. The cumulative mean and median values of KS distance between the intensity of pixels belonging to two different rings, generated over the whole image, have been estimated. The functions relating the mean and median values of KS distance d_{KS} versus the level l are linearly approximated in the forms

$$mean\_d_{KS} = \alpha_{0mean} + \alpha_{1mean} l + \varepsilon \quad (2)$$

$$med\_d_{KS} = \alpha_{0med} + \alpha_{1med} l + \varepsilon \quad (3)$$

where α_0 and α_1 are the regression coefficients corresponding to equations (2) and (3). The following KS parameters were taken for description of the image:

- $d_{KS}12$ (the mean and median values of KS distances between rings 1 and 2),
- $d_{KS}13$ (the mean and median values of KS distances between rings 1 and 3)
- $d_{KS}14$ (the mean and median values of KS distances between rings 1 and 4)
- the ratio $d_{KS}13/d_{KS}12$ in mean and median representation
- the ratio $d_{KS}14/d_{KS}12$ in mean and median representation
- the coefficient α_{0mean} and α_{0med} of the linear approximations (2) and (3)
- the slope coefficient α_{1man} and α_{1med} of the linear approximation (2) and (3)

In this way we obtained 14 descriptors following from the KS statistics.

3.1.2 Maximum subregion descriptors

The main idea in this method is to observe the process of disaggregating the image into smaller consistent subgroups by using thresholding at different values of bias [14]. The process of splitting is aimed to find the level of thresholding which provides the largest number of consistent subgroups. Many thresholding processes are performed on the image to achieve the goal.

In the searching procedure we apply the idea of quantile representation of pixel's intensity, i.e., 0.01, 0.02,.., 0.99. We search for the quantile q and its corresponding intensity threshold value th_q, which splits the image into the largest number of compact groups of pixels (the group is understood as the compact area isolated completely from the other pixels). The value of quantile q and its normalized threshold nth_q will form the diagnostic features.

The normalized threshold is defined as $nth_q = (th_q - f_1)\frac{255}{f_{99} - f_1}$, where f_1 is the lowest intensity level of the pixels corresponding to the first quantile and f_{99} the intensity level corresponding to 99th quantile. The third descriptor is defined in the form of the relative area of the largest compact subgroup of pixels in the image after thresholding. For two types of subimages after thresholding (the subimage of pixel intensity higher or lower than assumed threshold value) the number of these features is duplicated (six descriptors in total).

3.1.3 Percolation descriptors

The percolation descriptors are focused on differences in the complexity of the borders (smoothness, raggedness, etc.) of the structure formed by the pixels in the analyzed image. The image is first binarized into many subimages using different threshold values and then the "fire" is set in each segment [14,15]. In each iteration the pixels adjacent to the region under fire enlarge the fired area. The number of iterations needed to undear the whole image at different binarization thresholds are determined. This process is performed on the image resized to the dimension 1024×1024. In the first phase the image is covered by the horizontal and vertical lines located every 100 pixels. The fire, initiated in each node created by the crossing points of the horizontal and vertical lines, is spreading simultaneously in all directions (horizontal, vertical and diagonal). The process is repeated simultaneously on all subimages, which are obtained by the binarization made at different values of threshold. The more jagged image the longer is the fire duration. The threshold values are changed step by step in the intensity range [0 255] of the pixels, according to the decile steps from q=1 up to q=9. The fire duration (measured by the number of iterations) is registered for each value of threshold. The percolation descriptor of the image is assumed in the form of the weighted average measure q_w of quantiles, defined as follows

$$q_w = \frac{\sum_{i=1}^{9} q_i d_i}{\sum_{i=1}^{9} d_i} \quad (4)$$

where q_i is a quantile changing from 0.1 to 0.9 with step of 0.1 and d_i is the number of iterations of the fire at the threshold value corresponding to the ith decile. The segmentation is repeated many times on the subimages formed in thresholding process assuming the pixel intensity higher or lower than the assumed threshold value. This results in two numerical descriptors q_w corresponding to these two percolation processes.

3.1.4 GLCM texture descriptors

GLCM texture description is well known approach to characterization of the images. It is based on the co-occurrence matrix [15], which reflects the statistical relationships between the intensity of the neighboring pixels in the image. In this particular application we have limited texture characterization to four statistical descriptors of the co-occurrence matrix of the image. They include: local contrast of the image, which characterizes the intensity difference between a pixel and its neighbors over the whole image, correlation existing between different pixel pairs, energy representing the occurrence of repeated pairs in the image and homogeneity coefficient, the latter characterizing the distribution of elements in GLCM matrix.

3.1.5 Statistical descriptors of the image

The statistical descriptors of the image have been created directly on the basis of the pixel intensity level. They include the mean, median, standard deviation (std), kurtosis, minimum, maximum, cumulants of the second, third and fourth orders, the ratio of the difference of 0.75 and 0.25 quantiles related to the maximum of median (or the value 0.001 if the maximum is less than 0.001) and the ratio of std to maximum (or the value 0.001 if the maximum is less than 0.001). In this wat the total number of these descriptors is 11.

3.1.6 Self-similarity descriptors

This family of descriptors is the generalization of the box counting dimension applied to the grey scale image. The original ROI image resized to the dimension 1024×1024 is first covered by the grid of horizontal and vertical lines separating it into $s \times s$ small regions. In the next step the similarity of each region to the whole image is estimated. This is done by using statistics of Kolmogorov-Smirnov distance d_{KS} [17]. The higher the value of this distance the lower is the similarity index of the analyzed subregion to the whole image. After performing such calculations for all regions of the original image the new image of the size $n \times n$ is created. The ijth element of this image represents the similarity of this particular region to the whole image and is described by $y_{ij}=1-d_{KS}$. All similarity values are in the range of [0, 1].

Three different grids have been applied: 64×64, 128×128 and 256×256. Each of them generates the corresponding self-similarity images described by the matrices of the appropriate size. The following step is similar to the classical box-counting dimension of fractals [18]. The sum of elements corresponding to the appropriate matrices is calculated. At three applied sizes of the grid we get three pairs of points, representing the scale s (here s=64, 128, 256) and the sum $N(s)$ of the values of elements in the corresponding matrix. The linear regression in logarithmic scale is estimated for these results

$$\log_2(N(s)) = a\log_2(s) + b + \varepsilon \quad (5)$$

The slope a and intercept point b represent two descriptors of the image. The next 6 descriptors represent the mean value and standard deviation of the self-similarity matrices corresponding to the sizes: 64×64, 128×128 and 256×256. The total number of these descriptors is 8.

3.1.7 Segmentation based fractal texture descriptors

This method generates descriptors on the basis of multi-thresholding level Otsu algorithm and is called shortly SFTD [19]. The image is binarized using different pairs of upper and lower threshold values, which are selected by using the so called two threshold binary decomposition technique. Then, the recursive algorithm is applied to each image region until the desired number of threshold values n is obtained, where n is the user defined parameter. As a result the image is decomposed into a set of binary images. The more jagged edges of the segmented regions, the higher is their fractal dimension. Therefore, the box counting dimension of boundaries is a good candidate for being the numerical descriptor characterizing the image. Two additional descriptors are defined in the form of the size and mean gray level of the subimages. For n threshold values the number of descriptors is equal $3n$. In this application we have applied 12 threshold values selected in this way. As a result 36 numerical descriptors of the image have been defined.

3.1.8 Hilbert's descriptors

Hilbert space-filling, called Hilbert curve, is a continuous fractal space-filling curve providing a mapping between 1D and 2D space that preserves fairly well local regions of the image [20,21]. The 1-D Hilbert curve of the image represents pixel intensity in the points specified by the nodes as shown in Fig. 2, where we have limited representation for the grid of the size 8×8.

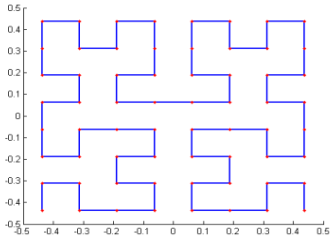

a)

22	23	26	27	38	39	42	43
21	24	25	28	37	40	41	44
20	19	30	29	36	35	46	45
17	18	31	32	33	34	47	48
16	13	12	11	54	53	52	49
15	14	9	10	55	56	51	50
2	3	8	7	58	57	62	63
1	4	5	6	59	60	61	64

b)

Fig. 2 The example of Hilbert curve (a) and the order of 64 pixels in 1-D vector representation of the image.

In this work the Hilbert representation of the mammogram containing 1024 elements has been used. As a result of such representation each analyzed image has been substituted by its vector form of the length 1024.

The family of descriptors is defined using the KS statistics estimated for two Hilbert sub-vectors traveling along the Hilbert curve with a step equal one. Both vectors have the length of 256 elements and occupy neighboring position in space. The KS distance d_{KS} for each position of these two vectors is estimated. On the basis of these distances and the corresponding significance levels p, the additional statistical descriptors are defined. They include the mean, median, std values of d_{KS} and p and also the corresponding ratio of std-to-mean calculated for both parameters. The set is supplemented by the values of 0.25 and 0.75 quantiles, their differences and the ratio of their difference related to maximum of median at the assumed significance level of 0.001 estimated for both parameters. In this way 16 Hilbert descriptors have been defined.

3.1.9 Multiscale Wavelet Transform descriptors

The Hilbert curve of the image is transformed into wavelet decomposition [22] and represented by the detailed coefficients on different levels and the residual signal on the last level of decomposition. Each detailed and residual signal has been characterized by 4 parameters: energy, variance, standard deviation, and waveform length. In this particular application db4 wavelet and 10 levels of decomposition have been used. The wavelet function type and number of decomposition levels have been selected after series of introductory experiments, in which Fisher discriminant measure was used to assess the quality of resulting descriptors. The procedure results in 11 waveforms representing 10 detailed coefficients and one residual signal. Since each waveform is characterized by 4 parameters we obtained 44 descriptors.

3.1.10 Wavelet packet descriptors

The wavelet packet decomposition was used to form the next set of descriptors [23]. The wavelet packet decomposition was applied also to the Hilbert vector form of the image. The db4 wavelet family and two levels of decomposition were used in the numerical experiments. As a result 16 vectors representing the details on four levels and the residual vectors for the last fourth level have been obtained. Each vector is characterized by the energy of its elements, i.e. $E_k = \sum_i \left(x_i^{(k)}\right)^2$ for k=1, 2,…, 16, where $x_i^{(k)}$ represents the value of element in i-th position in kth detail or residual vector. These values create the set of 16 wavelet descriptors.

3.2. Feature selection

The total number of descriptors defined in the previous sections is equal 157. However, not all of them represent the equally good features in class discrimination. Therefore, the selection process is needed, which should select the set of the best diagnostic features representing the highest class recognition ability. Sequential forward and backward selection method [17, 24] has been applied. This approach was due to high effectiveness and relatively quick performance. As a result of its application the specific set of optimal features is generated. This is in contrast to other methods based on other informative or correlation measures.

The individual descriptors are added and removed from the actual feature set in the selection process. After including or removing the feature the newly created set of features is checked for the class prediction accuracy. If the added or removed descriptor has increased the accuracy of the resulting set, the operation is accepted, otherwise it will be discarded [17]. In the process of checking the class discrimination ability of the actual feature set the support vector machine of radial kernel was used as the classifier. For every candidate feature subset the sequential feature selection was applied using 10-fold cross-validation, by repeatedly calling function with different training subsets of learning data and the changing validation subset of data. As the result of such selection process we get the logical vector indicating which features are finally chosen by the selection procedure.

Only 39 diagnostic features out of 122 descriptors generated in the initial image description have been left after this selection process. The composition of the selected feature contained the representatives of all types of descriptions. Among the selected features there were 9 representatives of multiscale wavelet transformation, 8 Hilbert descriptors, 5 wavelet packet descriptors, 4 SFTA descriptors, 3 percolation descriptors, 3 statistical descriptors, 3 fractal descriptors, 2 Haralick texture descriptors, one maximum subregion and one KS descriptor.

3.3. Results of numerical experiments

The dataset was split into 10 subsets, each containing the same proportion of both classes, related to their populations in the database. Nine parts of samples are used in the feature selection and learning the SVM classifier and the last one used for testing the learned system. The same experiments have been repeated ten times, exchanging the testing and learning subsets. To balance the number of classes in each experiment the normal class was split into four parts, each associated with the same abnormal cases and the results were averaged. The training and testing sets have been chosen randomly from the data base.

Different classifiers, including SVM, multilayer perceptron, decision tree and random forest have been tried in the introductory experiments. However, the best results have been obtained for SVM of the radial Gaussian

kernel $K(\mathbf{x},\mathbf{x}_i)=\exp\left(-\gamma\|\mathbf{x}-\mathbf{x}_i\|^2\right)$ of γ=0.1 at application of the regularization constant C=1000, and only these results will be presented here. These parameters have been selected after introductory experiments performed on a small set of data using the set of predefined values for C and γ. The parameters leading to the best results of recognition have been selected. The classification experiments have been done for the whole set of features and for the reduced set of features created by the stepwise fit.

Table 1 summarizes the statistical classification results for the testing data achieved by the SVM for all descriptors and after their selection. The first number represents the mean value and the term after ± sign the standard deviation, both obtained in the repeated 10-fold cross validation experiments. We have applied this procedure, since it is the approach regarded as the most objective in estimation of the quality of the applied model. This id due to the fact, that all data take simultaneously part in learning and testing stages.

Table 1
The results of mammogram recognition using classical neural approach

	All features	Selected features
Accuracy	78.73%± 1.96	81.01%± 2.36
Sensitivity	79.73%± 1.53	82.48%± 1.97
Specificity	77.73%± 1.79	79.63%± 2.02

4. Deep learning in application to mammogram recognition

Deep learning is the novel stream of research integrating the process of self-organizing feature selection and final classification of the images [25,26]. In this research we have applied the convolutional neural network (CNN) as a work horse. The important problem in this approach is the limited number of images, representing the abnormal cases. To increase the information of the class differences among the analyzed mammograms the additional preprocessing of the images has been proposed. It was done by applying nonnegative matrix factorization (NMF) and the statistical self-similarity of the images. Thanks to this additional view on the mammograms the diagnostic information contained in the original data base has been enhanced.

4.1 Image representation using NMF

The non-negative matrix factorization is a decomposition technique representing the given matrix **P** by two matrices **W** and **H,** both of the non-negative elements [27, 28], i.e., **P=WH**. The columns of **W** represent the basis vectors and the columns of **H** the encodings associated with them. Assume the matrix **P** is composed of the column vectors of the length *N* and *M* the number of such vectors. The matrices **W** and **H** are of the size *N*×*r* and *r*×*M*, respectively, where the value of *r* is the factorization rank adjusted by the user (usually (*N*+*M*)*r*<*NM)*.

The NMF factorization will be performed here to enrich the representation of the mammographic images and to enhance the difference between mammograms representing normal and abnormal cases. All analyzed mammographic images are represented in the vector Hilbert form. They are grouped in the matrix **P**.

The NMF operation will be performed on the set of mammograms representing only normal cases, since these images are more alike to each other. Only half of vectors belonging to the normal class has been used in this step of processing. According to NMF procedure the matrix **P** is decomposed into **W** and **H** of non-negative elements. The factorization means, that *i*th vector $\mathbf{p}_i$ (the *i*th column of **P**) can be expressed as the weighted sum of basis vectors and it might be presented in Matlab notation [17] as following

$$\mathbf{p}_i=\sum_{j=1}^{r}\mathbf{W}(:,j)\mathbf{H}(j,i) \tag{6}$$

The whole set of original mammographic images representing normal and abnormal cases is converted to the NMF factors and then reconstructed using only limited number *r* of the basis vectors. In these investigations we have applied only 10 basis vectors in reconstruction (*r*=10). Since the NMF decomposition was performed only on the normal cases, such reconstruction will represent better the images of this class. The abnormal cases reconstructed by the basis vectors obtained in NMF decomposition of only normal cases, will show larger discrepancy to the original ones. This way the differences between normal and abnormal cases have been increased. Thanks to it the recognition of classes will be easier.

4.2 Statistical self-similarity for the image representation

The next type of transformation applied to the original images is created using the so-called statistical self-similarity. These images are defined on the basis of statistics of the pixel intensity distribution in regions, which are small in comparison to the whole image. In the first stage of processing the image is resized to the dimension 1024×1024 pixels and then split into small 5×5 compact overlapping regions. This way the original mammographic image is represented by 256×256 small sub-images. In the next step the similarity of these sub-images to the whole image is measured using the Kolmogorov-Smirnov d_{KS} distance [17]. As a result the small subregions are represented by the single values equal to 1-d_{KS}, with the range between 0 and 1. The lower the value of KS, the more similar the sub-image to the whole image is. In final stage, the set of 256×256 KS images is scaled back to the original dimension of 128×128. Such transformation of images increases the differences between representatives of various classes.

4.3 Convolutional neural network in mammogram recognition

CNN model is a very complex nonlinear structure, exploiting the high-level abstraction by using multiple hidden layers [25, 26]. These layers are able to extract and identify different levels of details of the images. In the higher layers the more abstract concepts are learned on the basis of the previous patterns extracted by the lower layers. The layer is composed of group of neurons, performing the role of locally connected filters. Each neuron receives input signals from a set of compact units located in a small neighborhood of the previous layer. The neurons extract the elementary features, such as blobs, edges, crossings of edges, end points, corners, etc. The local reception field of each neuron is moved along all pixels of the image with the step (stride) defined by the user.

The features combined by the subsequent layers create finally fully connected layer, representing the input signals to the output classification layer. The output signals of this layer are generated by the softmax units and form the final class recognition. Softmax layer calculates the output value based on the multinomial logistic regression [26], representing the probability of membership of the actual input vector to the appropriate class. The number of units in Softmax layer is equal to the number of classes. The class of the highest probability is taken as the final winner. The detailed description of CNN can be found in [25].

In this paper the CNN containing three convolution layers and two fully connected layers has been found as the most successful [12]. The details of the following layers are as following.

- The first convolution layer structure: 32 filters of dimension 5×5 with zero padding 2×2 and stride 1×1; Max pooling of the size=3×3, zero padding=0×0, stride=2×2; Rectified Linear Unit layer.
- The second convolution layer structure: 32 filters of dimension 5×5, zero padding 2×2, stride 1×1; Average pooling of the pooling size=3×3 with zero padding=0×0, stride=2×2; Rectified Linear Unit layer.
- The third convolution layer structure: 64 filters of dimension 5×5 with zero padding 2×2 and stride 1×1; Average pooling of size=3×3 with zero padding=0×0, stride=2×2; Rectified Linear Unit layer.
- The first Fully Connected Layer: 64 neurons with Rectified Linear Units.
- The second Fully Connected Layer contains two neurons (dependent on number of recognized classes) with Softmax. It performs the role of final classification.

The general organization of the CNN system for recognition of classes of mammograms is presented in Fig. 3 [12].

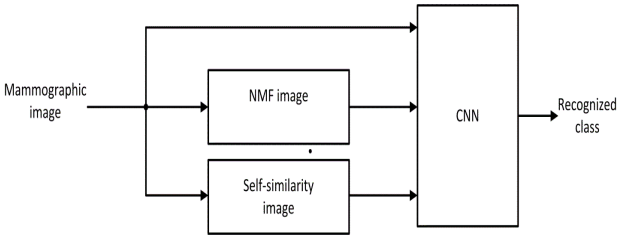

Fig. 3 The deep learning system used in mammogram recognition.

The CNN is supplied by three images representing the analyzed mammograms: the original mammographic image, the image reconstructed on the basis of NMF and the transformed image reconstructed on the basis of the self-similarity principle. Thanks to these additional transformations of the mammograms more information regarding the structure of the analyzed images is delivered to CNN. At the same time the number of input data is also triplicated. The information enhanced in this way significantly increases the probability of correct classification.

4.4. Results of numerical experiments

The numerical experiments of mammogram recognition using CNN have been performed on the same samples of mammograms in DDSM database as used in the previous section. The aim was to recognize the normal cases (class 1) from abnormal (benign and malignant jointed together) representing class 2. The experiments have been performed using 10-fold cross validation organized in the same fashion as in the classical approach. Only half of the normal cases in the learning sets have been used in NMF decomposition to get the basis vectors of **W** used in the reconstruction of all mammographic images.

The procedure of the final class recognition was performed in the following way. The continuous output of the classifier in the learning mode (before binarization) was subject to the dynamic thresholding at different values of threshold. The threshold generating the highest quality measure for the learning data was fixed and applied in testing the remaining validation data (10% of data in each run of cross validation procedure). The quality measure, which was taken into account in this step included the value of AUC of the receiver operating characteristic. The maximized AUC measure is a good compromise between the sensitivity (ability to discover the minority class) and specificity (ability to discover the majority class) of the recognition system.

Table 2 presents the detailed results of recognition of mammograms obtained in the testing mode of the 10-fold cross validation [12]. The results of recognition of normal cases from abnormal are presented in the form of sensitivity, specificity and average accuracy. The sensitivity of recognizing the abnormal cases from normal was equal 82.82% and specificity 86.59%. The obtained accuracy is somewhere in the middle of them (85.83%. The obtained area under ROC curve AUC=0.919. These

results belong to the best already reported for this large DDSM database.

Table2

The results of numerical experiments of mammogram recognition using CNN

Sensitivity	Specificity	Accuracy
82.82%± 0.95	86.59%± 1.12	85.83%± 1.08

Comparison with the classical results presented in Table 1 shows evident advantage of the deep learning approach. All quality measures have been increased in a significant way. To assess the importance of inclusion the NMF and self-similarity images in recognition process the additional experiments have been performed using only the original images of mammograms. The obtained AUC value for recognition of abnormal from normal cases was reduced to AUC=0.88. According to *ranskum* test at 5% significance level this difference is statistically significant.

5. Comparative study

The problem of mammogram recognition was studied in many papers. However, most of them used either different data base or very limited images selected from DDSM. Different quality measures have been also applied in presentation of the results. Therefore it is difficult to present the comparison to all these works in an objective way. We will limit here the comparison to the papers, which have used the same DDSM data base.

The paper [7] has considered very small set of 410 mammograms of DDSM database and the overall accuracy achieved by authors was 87% with 88.6% sensitivity and 78.6% specificity. Due to small number of samples these results are not fully credible. The quality measure of solution in the form of AUC value was presented in the papers [8] and [28]. The AUC value of 0.789 for 600 cases was reported in [8] and 0.871 for 1000 screening mammograms in [28].

In [30] deep CNN approach to recognition of normal from abnormal mammograms on very large data base from Netherlands, containing over 44000 mammographic views has been presented. The results are represented by ROC curve. The best AUC with the augmentation (context, location, patient information) and manual feature support was AUC=0.941. The best results without augmentation was AUC=0.929.

In [31] the results for DDSM declaring 85% of accuracy and AUC=0.91 have been presented. They were obtained using Google Le Net system and ensemble of 100 parallel networks.

The results for DDSM base presented in [32] have covered 1057 malignant and 1397 benign cases. They were concentrated on ROC and declared the best value of AUC=0.82.

In [33] the DDSM for more than 6000 mammographic images and ZMDS (1739 mammograms) have been considered. The best results for images declared AUC=0.922, sensitivity 0.901 and specificity 0.783.

Our best average accuracy in recognizing abnormal cases (malignant plus benign versus healthy) for the whole images in DDSM data base was 85.83%, sensitivity 82.82%, specificity 86.59% and AUC=0.919. The only recent results presented also for the whole DDSM data base (2003 abnormal and 9215 normal mammograms) are given in [11]. The accuracy in abnormality detection (malignant plus benign versus healthy) reported in this paper by using the curvelets for the same DDSM data base was in the range from 81.3% to 86.4% depending on the applied feature set. However, the sensitivity, specificity and AUC were not given. It is difficult to assess the quality of their solution on the basis of only accuracy value, since it is very easy for this unbalanced data set (2003 abnormal and 9215 normal mammograms) to obtain high accuracy on the cost of sensitivity. In our additional experiments by applying the accuracy as the quality measure of an ensemble, we have obtained the average accuracy equal 89.4%, however, on the cost of sensitivity which has dropped to only 69.5%.

4 Conclusions

The paper has presented the comparative analysis of the classical and deep learning approach to the recognition of abnormal from normal cases on the basis of the mammogram images. In the classical approach the extended set of numerical descriptors has been proposed. They were defined on the basis of different principles of image characterization and included representation of the image by Hilbert form and corresponding descriptors, Kolmogorov-Smirnov statistics, maximum subregion principle, percolation theory, fractal texture descriptors as well as application of wavelet and wavelet packets. Thanks to so many applied methods, different points of view on the image were considered in pattern recognition. However, in spite of such rich descriptive representation of the images and application of the efficient SVM classifier, the results were inferior in comparison to the application of deep learning approach, enhanced by the non-negative matrix factorization and self-similarity of the images.

The most important advantage of deep learning for mammogram recognition is the relatively simple way of preparation of input data to the convolutional neural network. The diagnostic features are self-defined in an unsupervised approach to the process of CNN learning. However, to get good results of recognition large number of learning samples should be used. The NMF and self-similarity transformations have not only enhanced the information of the image details but also increased the population of samples taking part in learning. Better results of recognition might be expected after further increasing the population of the original images of the mammograms.

The additional investigations are needed to increase the accuracy to the level acceptable for everyday use in medical practice. The next investigations will explore

both approaches. The classical one will be directed to apply more classifiers arranged in an ensemble to increase the diversity of principles on the basis of which the final decision is made. In the case of deep learning the new perspective are open now by transfer learning [26]. The more specialized ways of learning the hidden neurons in CNN will be studied. In both cases the accuracy of image recognition might be increased by applying the larger data base of abnormal cases.

REFERENCES

[1] J. Ferlay, I. Soerjomataram, R. Dikshit, S. Eser, C. Mathers, M. Rebelo and F. Bray, "Cancer incidence and mortality worldwide: sources, methods and major patterns in GLOBOCAN". *International Journal of Cancer* 136(5), E359-E386 (2012).

[2] H. Nelson, K. Tyne, A. Naik, C. Bougatsos, B. Chan, P. Nygren and L. Humphrey L, "Screening for breast cancer: Systematic evidence review update for the U. S. preventive services task force", *Ann. Intern. Med.* 151(10), 727-W242 (2009).

[3] S. Hofvind, G. Ursin, S. Tretli, S. Sebuodegard and B. Moller, "Breast cancer mortality in participants of the Norwegian breast cancer screening program", *Cancer* 119(17), 3106-12 (2013).

[4] A. Jalalian, S.B. Mashohor, H.R. Mahmud, M.I. Saripan, A.R. Ramli and B. Karasfi, "Computer-aided detection/diagnosis of breast cancer in mammography and ultrasound" *Clinical Imaging* 37, 420-426 (2013).

[5] Z. Wang, Q. Qu and G. Yu, "Breast tumor detection in double views mammography based on extreme learning machine", *Neural Computing and Applications* 27(1), 227-240 (2016)

[6] I. Christoyiani, A. Koutra, E. Dermata and G. Kokkinakis, "Computer aided diagnosis of breast cancer in digital mammograms", *Computerized Medical Imaging and Graphics* 26, 309-319 (2002).

[7] B.K. Elfarra and I.S. Abuhaiba, "New Feature Extraction Method for Mammogram Computer Aided Diagnosis", *Intern. Journal of Signal Processing, Image Processing and Pattern Recognition* 6(1), 1-81 2013.

[8] M. Mazurowski, J. Zurada and G. Tourassi, "Selection of examples in case-based computer-aided decision systems", *Physics in Medicine and Biology* 53, 6079–6096 (2008).

[9] M. Lobbes, M. Smidt, K. Keymeulen, R. Girometti, C. Zuiani, R. Beets-Tan, J. Wildberger and C. Boetes, "Malignant lesions on mammography: accuracy of two different computer-aided detection systems", *Clinical Imaging* 37, 283-288 (2013).

[10] S. Leon, L. Libby Brateman, J Honeyman-Buck and J.Marshall, "Comparison of two commercial CAD systems for digital mammography", *Journal of Digital Imaging* 22(4), 421–423 (2009) doi: 10.1007/s10278-008-9144-x.

[11] S. Dhahbi, W. Barhoumi and E. Zagrouba, "Breast cancer diagnosis in digitized mammograms using curvelet moments", *Computers in Biology and Medicine* 64(1), 79-90 (2015).

[12] B. Swiderski, J. Kurek, S. Osowski, M. Kruk and W. Barhoumi "Deep learning and non-negative matrix factorization in recognition of mammograms", in *Proc. SPIE 10225B, Eighth Int. Conf. Graphic and Image Processing*, (2016) doi:10.1117/12.2266335.

[13] M. Heath, K. Bowyer, D. Kopans, R. Moore and P. Kegelmeyer, "The digital database for screening mammography", in: *Digital Mammography*, Springer, Netherlands, 457-460 (1998).

[14] B. Swiderski, S. Osowski., J. Kurek, M. Kruk, I. Lugowska, P. Rutkowski and W. Barhoumi, "Novel methods of image description and ensemble of classifiers in application to mammogram analysis", *Expert Systems with Applications* 81, 67–78 (2017).

[15] D. Stauffer, *Introduction to percolation theory*, Taylor & Francis, London, 1985.

[16] R. Haralick and L. Shapiro, Image segmentation techniques. *Computer Vision. Graphics and Image Processing* 29, 100–132 (1985).

[17] *Matlab user manual*, MathWorks, Inc. Natick, USA, 2017.

[18] M. Schroeder, *Fractals, Chaos, Power Laws*. W.H. Freeman and Company, New York, 2006.

[19] B. Moon, H.V. Jagadish, C. Faloutsos and J.H. Saltz, "Analysis of the clustering properties of the Hilbert space-filling curve", *IEEE Transactions on Knowledge and Data Engineering* 13(1):124–141 (2001) doi:10.1109/69.908985

[20] A. Costa, G. Humpire-Mamani and A. Traina, "An efficient algorithm for fractal analysis of textures", in *Proc. 25 SIBGRAPI Conference on Graphics, Patterns and Images*, 39-46 (2012).

[21] M. Jiang, S. Zhang, H. Li and N. Metaxas, "Computer-aided diagnosis of mammographic masses using scalable image retrieval", *IEEE Transactions on Biomedical Engineering* 62(2), 783-792 (2015).

[22] I. Daubechies, *Ten lectures on wavelets*, SIAM, Philadelphia, 1992.

[23] R.N. Khushaba, S. Kodagoa, S. Lal and G. Dissanayake, "Driver drowsiness classification using fuzzy wavelet packet based feature extraction algorithm", *IEEE Transaction on Biomedical Engineering* 58(1), 121-131 (2011).

[24] J. Kurek, M. Kruk, S. Osowski, P. Hoser, G. Wieczorek, A. Jegorowa, J. Górski, J. Wilkowski, K. Śmietańska and J. Kossakowska, "Developing automatic recognition system of drill wear in standard laminated chipboard drilling process", *Bulletin of the Polish Academy of Sciences Technical Sciences*, 64(3), 633-640 (2016).

[25] I. Goodfellow, Y. Bengio and A. Courville, *Deep learning*, MIT Press, Massachusetts, USA, 2016.

[26] A. Krizhevsky, I. Sutskever and G. Hinton, "Image net classification with deep convolutional neural networks", Advances in Neural Information Processing Systems 25, 1-9 (2012).

[27] D. Lee and H. Seung, "Learning the parts of objects by non-negative matrix factorization", *Nature* 401, 788-791 (1999).

[28] A. Cichocki, R. Zdunek, A.H. Phan and S.I. Amari, *Nonnegative matrix and tensor factorizations: applications to exploratory multi-way data analysis and blind source separation*, Wiley, New York, 2009.

[29] J.J. Fenton, S.H.Taplin, P.A. Carney, et al. "Influence of computer-aided detection on performance of screening mammography", *New England Journal of Medicine* 356, 1399-1409 (2007).

[30] T. Kooi, G. Litjens, "Large scale deep learning for computer aided detection of mammographic lesions", *Medical Image Analysis*, 35, 303-312 (2017).

[31] D. Yi, R.L. Sawyer, D. Cohn III, J. Dunnmon and C. Lam, „Optimizing and visualizing deep learning for benign/malignant classification in breast tumors", *29th Conf. NIPS 2016*, arXiv preprint, arxiv.org (2017.

[32] R.K. Samala, H.P. Chan and L.M. Hadjiiski, „Multi-task transfer learning deep convolutional neural network: application to computer-aided diagnosis of breast cancer on mammograms", *Physics in Medicine & Biology* 62, 8894-8908 (2017).

[33] P. Teare, M. Fishman, O. Benzaquen and E. Toledano, "Malignancy Detection on Mammography Using Dual Deep Convolutional Neural Networks and Genetically Discovered False Color Input Enhancement", *Journal of Digital Imaging* 30, 499-505 (2017).